Self-Tuning High-Voltage High-Frequency Switching Power Amplifier for Atmospheric-Based Plasma Sterilization

Raul Andres Chinga, *Student Member, IEEE*, Jenshan Lin, *Fellow, IEEE*, and Subrata Roy

***Abstract*— In this paper, the implementation of a power supply for the generation of plasma, with the purpose of sterilizing a surface, is presented. A power supply based on a Class-E switching amplifier is proposed. This switch-mode amplifier is capable of producing a high-voltage and high-frequency output for plasma generation. In addition, a feedback mechanism is used to handle load variation. This is achieved through the characterization of the load at high voltages while generating plasma. Portability of the system is the primary goal of this paper. Thus, the implementation of a miniaturized circuit capable of achieving high efficiency and low power consumption at the same time is critical. The design and implementation of the complete battery-powered system, as well as the simulation and measurement results are discussed.**

***Index Terms*— Class-E, dielectric barrier discharge (DBD), feedback, high voltage, plasma, sterilization.**

I. Introduction

DIELECTRIC barrier discharge (DBD) at atmospheric pressure has potential of becoming a new practical and effective method of sterilization. Sterilization technology has broad applications, from medical devices to food preparation equipment. When plasma is generated, radicals are formed, such as ozone, along with heat, and UV light. It is the combination of these components that makes sterilization possible. Several studies have been conducted on the killing potential of plasma over different bacteria and spores [1]–[8]. Mastanaiah *et al.* [1], [2] have obtained results of complete sterilization within 60–120 s, highly emphasizing the effectiveness of plasma as a more efficient mechanism than autoclaving, for instance, which takes about 1 h.

This paper presents a design of portable electronics that can generate DBD plasma with battery operation. In general, the proposed technique can be applied to other applications generating high voltages on capacitive loads.

The DBD plasma is produced when an alternating high voltage is applied on two electrodes separated by a dielectric. This high voltage results in strong electric fields that generate electrical discharge. Several power amplifier (PA) designs capable of generating high voltage outputs for ozone and plasma generation have been reported [9]–[21]. Alonso *et al.* [9] present a topology similar to an ignition circuit that can generate a high voltage output. It also indicates that the efficiency of the PA is 50%. Since the total power provided to the load is only 1 W, this power loss is not significant. However, one issue not discussed in [9] is the current spike generated when the transistor switches OFF, causing losses and adding stress on the transistor.

Ponce-Silva *et al.* [10] and Facta *et al.* [11] show a topology which is based on a modified Class-E topology. The Class-E topology is introduced in [22] and further analyzed in [23] and [24]. Both [10] and [11] have developed systems operating in the kHz range (27 and 8 kHz, respectively). However, [10] requires a large inductor on the load side. This inductor resonates with the capacitive load to produce a high-voltage sinusoidal waveform. To decrease the inductor size, Ponce-Silva *et al.* [10] added a capacitor in shunt with the load to increase the overall load capacitance, thus decreasing the resonating inductor requirement. This method is not desirable because it requires two additional components and increases power loss. On the other hand, [11] does not use a resonating inductor. Instead, it operates at a frequency close to the resonance of the transformer and the capacitive load. Similarly, Petreus *et al.* [12] present a plasma torch generator using a Class-E amplifier. The frequency of operation is 13.56 MHz and has an output up to 2 kV. However, this system is large in size due to the current requirement of the application. Other topologies like current-fed push-pull resonant inverters or full-bridge inverters presented in [13]–[17] are also used to produce high voltage across capacitive loads. Alonso *et al.* [14] are particularly interesting because it maximizes an efficient high voltage output by resonating the transformer along with the load. However, these designs require two or four transistors and increase complexity. Other works involve high voltage pulsed generators, [18]–[20], which are capable of generating plasma. However, for this application, a sine wave is desired. Finally, [21] provides a summary of different circuit topologies used for ozone generation. It compares various high voltage sources and their respective ozone concentrations generated.

The purpose of the plasma sterilizer is to kill bacteria on the surface. Most of the time, the surface will contain small quantities of liquid due to contamination. Once plasma is generated across the surface, this liquid will evaporate

Manuscript received July 28, 2013; revised January 25, 2014; accepted May 17, 2014.

R. A. Chinga and J. Lin are with the Department of Electrical and Computer Engineering, University of Florida, Gainesville, FL 32611 USA (e-mail: ralndres@ufl.edu; jenshan@ufl.edu).

S. Roy is with the Department of Mechanical and Aerospace Engineering, University of Florida, Gainesville, FL 32611 USA (e-mail: roy@ufl.edu).

Color versions of one or more of the figures in this paper are available online at http://ieeexplore.ieee.org.

Digital Object Identifier 10.1109/TPS.2014.2328900

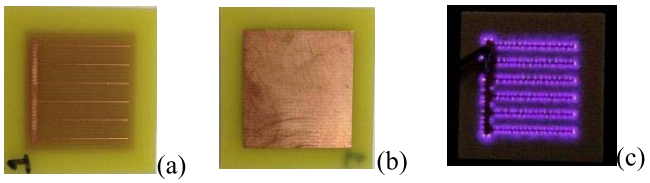

Fig. 1. (a) and (b) Front and back electrodes of the SSD. (c) Electrode with DBD plasma on it.

gradually, causing the amplifier load impedance to change during plasma sterilization, which presents a challenge to the amplifier design. This change of impedance is unique to this application and has not been addressed in previous works. The only change of impedance mentioned has been the capacitance added by plasma, but not by the contamination of the surface.

Using [9]–[21] as a starting point, the rest of this paper discusses the design of the PA step by step. Section II presents a mechanism to model the large-signal load impedance with plasma generated, as well as the variation due to contamination. In Section III, the PA is then designed using the parameters extracted from the modeling. Section IV shows the implementation of the circuit. The handling of varying load by the PA is also demonstrated in this section. The automation of the system is presented in Section V, which emphasizes the challenges of implementing feedback control. Finally, Section VI presents a brief summary and conclusion of this paper.

II. Modeling of Varying Load

In this paper, the plasma is produced at atmospheric pressure. The load of the system consists of two metal electrodes separated by a dielectric (Rogers 4003C) of 1.54-mm thickness, referred to as the self-sterilizing device (SSD). The voltage required to achieve the discharge, typically a few kilovolts, is determined by the distance between the electrodes, the dielectric constant, and the pressure. The plasma discharge is extinguished when the electric current is terminated or the electric field collapses [1]. The size of the SSD shown in Fig. 1 is $1.5'' \times 1.5''$ (more detailed explanations on the design of the SSD can be found in [1] and [2]).

Ponce-Silva *et al.* [10] presented a device model, which is described in detail in [25]. Using this technique, the SSD is modeled as a parallel *RC* equivalent circuit (C_P and R_P). The resistor models the power dissipated when generating ozone, heat, and UV light, while the capacitor represents the equivalent capacitance of the dielectric and the discharge gap. There are other circuit models for plasma as the one presented in [26]; however, it adds complexity, which makes it more difficult to analyze. The model in [25] is sufficient for the analysis of this paper.

The values of C_P and R_P are determined using

$$C_P = \frac{I_o}{2\pi f V_{\text{SSD}}} \tag{1}$$

$$R_P = \frac{V_{\text{SSD}}}{2\pi f Q_o} \tag{2}$$

$$P_{\text{AV}} = \frac{V_{\text{SSD}}^2}{2R_P}. \tag{3}$$

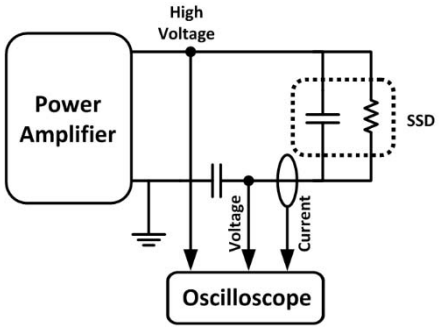

Fig. 2. Setup used to extract I_O and Q_O. These determine C_P and R_P to model SSD as a function of frequency and voltage.

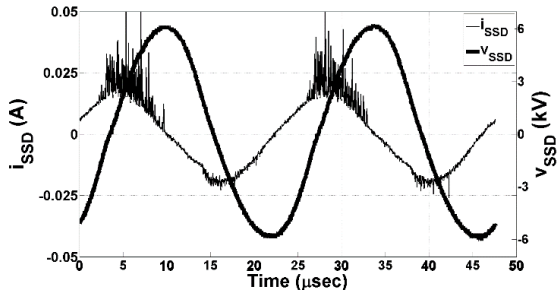

Fig. 3. SSD with DBD plasma.

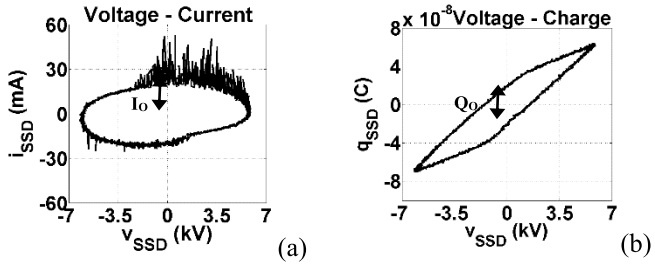

Fig. 4. Lissajous diagrams. (a) Voltage–current and (b) voltage-charge used to extract I_{O} and Q_{O} values, respectively.

To evaluate C_P and R_P, V_{SSD} (the amplitude of the voltage across the SSD), I_{O} and Q_{O} (the current and charge when $v_{\text{SSD}} = 0$, respectively, in Fig. 4) must first be determined. These are extracted by using the setup shown in Fig. 2. A high voltage probe (Tektronix P6015A) is used to record the voltage across the SSD, a regular voltage probe (Tektronix P2220) measures the voltage drop across the series capacitor C, while the current is measured using a high voltage current probe (Bergoz CT-D1.0-3).

The value of the series capacitor, C, is selected so as to be much larger than the SSD capacitance. The purpose of this capacitor is to determine the charge of the SSD without loading the system [25]. Fig. 3 shows the voltage v_{SSD} across the SSD as well as the current i_{SSD} flowing through it. As illustrated, the current has random spikes which are caused by the ionization of gas molecules in the air and the discharge of radicals and photons. Fig. 1(c) shows the SSD with the plasma being generated on the electrode.

Following the procedure presented in [25], the Lissajous diagrams, voltage–current, and voltage-charge are plotted, from which I_O and Q_O are extracted. Using Fig. 4

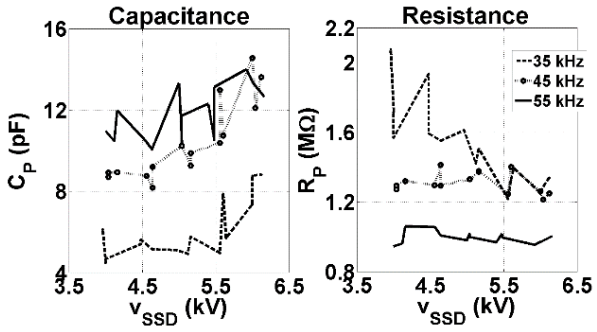

Fig. 5. Equivalent plasma capacitance C_P and resistance R_P as a function of applied voltage and frequency.

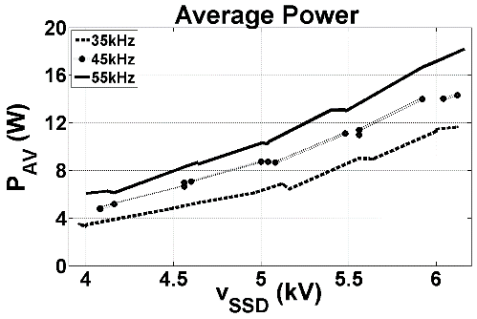

Fig. 6. SSD average power P_{AV} as a function of applied voltage and frequency.

and (1) and (2), C_P and R_P are evaluated. Fig. 5 shows the variation of C_P and R_P as v_{SSD} and the operating frequency is swept from 4–6 kV and 35–55 kHz, respectively. It is shown that C_P increases as the voltage increases and the operating frequency increases, while R_P follows the opposite trend. Fig. 6 shows the average power dissipated by the SSD. This is evaluated using (3). It should be noted that C_P, R_P, and average power P_{AV} do not follow a smoother trend due to the current spikes generated by plasma. From this, it is concluded the system needs to be tuned every time when the frequency or the voltage is changed (which is expected).

Furthermore, the load variation due to contamination needs to be considered. As described earlier, the purpose of the plasma sterilizer is to kill bacteria located on the surface of the SSD. Such contamination is represented as the presence of some liquid on the surface. As the plasma is generated across the SSD, the bacteria and the liquid evaporate, gradually changing the impedance. To measure the actual impedance change, three sets of experiments are performed.

1) 40 μL of three different types of liquid are applied on the surface of the SSD, spread out evenly. Three mediums are used: water, salt water, and serum. This experiment determines how much the impedance variation differs using different mediums.
2) 20, 40, 60, and 80 μL of tap water only are applied to the surface of the SSD. This experiment determines how much the impedance variation differs by applying different volumes of liquid.
3) Experiment 2 is repeated but without spreading out the liquid, just applying it as a single drop at the center of the SSD (Fig. 7).

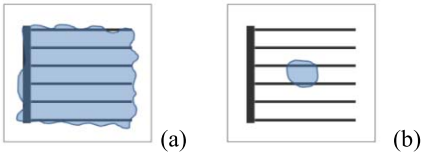

Fig. 7. SSD liquid tests. (a) Covering the entire surface. (b) Single drop.

TABLE I
IMPEDANCE VARIATION DUE TO DIFFERENT MEDIUMS

Liquid	SSD Impedance	SSD w/ 40 µL	Impedance Change	Percentage Change
Water	8 pF	19.4 pF	11.4 pF	144%
Salt Water	8 pF	20.6 pF	12.6 pF	159%
Serum	8 pF	21.1 pF	13.1 pF	166%

TABLE II
IMPEDANCE VARIATION DUE TO DIFFERENT VOLUMES OF LIQUID (WATER) EVENLY SPREAD OVER THE SSD SURFACE

Volume	SSD Impedance	SSD w/water	Impedance Change	Percentage Change
20 µL	6.26 pF	17.34 pF	11.1 pF	177%
40 µL	6.25 pF	17.53 pF	11.3 pF	180%
60 µL	6.20 pF	17.43 pF	11.2 pF	181%
80 µL	6.24 pF	17.30 pF	11.1 pF	177%

TABLE III
IMPEDANCE VARIATION APPLYING A SINGLE DROP OF LIQUID (WATER)

Volume	SSD Impedance	SSD w/ water	Impedance Change	Percentage Change
20 µL	6.20 pF	7.56 pF	1.36 pF	22%
40 µL	6.16 pF	7.44 pF	1.28 pF	21%
60 µL	6.18 pF	7.50 pF	1.32 pF	21%
80 µL	6.16 pF	7.22 pF	1.10 pF	17%

(Note: 20 μL is the volume of a single drop of liquid.) Using the HP 4192A LF Impedance Analyzer, the impedance across the SSD is measured for these three cases.

As shown in Table I, the impedance changes using three different liquids are approximately the same. The change ranges from 144% to 166%. Table II shows the impedance change applying different volumes of water. For this experiment, the percentage change ranged from 177% to 181%. On the other hand, the impedance variation due to a single drop of liquid with different volumes is small. This is shown in Table III. From these experiments, it is concluded that the impedance change depends on the way the liquid is placed but not the volume of the liquid.

The model of large-signal load impedance and its variation during sterilization is critical to the PA design, which is discussed in Section III.

III. PA CIRCUIT

Before designing the PA, the operating frequency, output voltage, and power delivered are determined first.

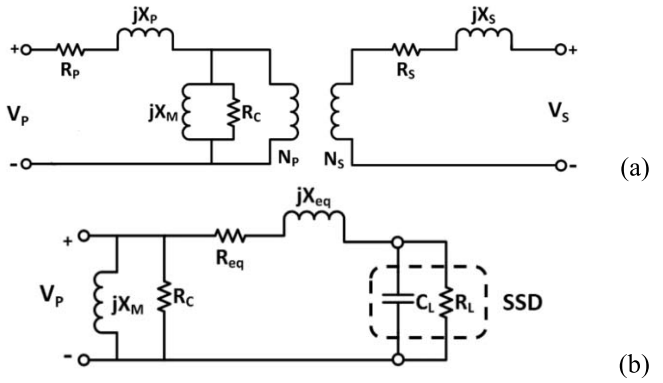

Fig. 8. (a) Transformer equivalent circuit. (b) Simplified transformer equivalent circuit referred to its primary side with load connected to its secondary side.

To obtain the highest voltage swing across the SSD with the least amount of power, the load is resonated with the transformer [11]. Fig. 8(a) shows the nonideal transformer model. The leakage flux is modeled by primary and secondary inductors (L_P and L_S) while the magnetizing inductance is modeled by L_M. The core-loss is modeled by R_C, while R_P along with R_S represent the copper losses. Its simplified form with the load connected to the secondary side is shown in Fig. 8(b), where the leakage inductance has been replaced by a single inductor, L_{eq}, and the copper losses have been replaced by R_{eq}. The transformer has been removed but X_{eq} and R_{eq} have been adjusted accordingly to take into account the number of turns ratio, as demonstrated in (4).

Resonance is achieved when the reactance of the load along with X_{eq} equals the conjugate of X_M (5). Equation (6) shows the frequency, ω, at which resonance takes place. The values of L_M and L_{eq} (leakage) are extracted from the open-circuit and short-circuit tests, respectively. The capacitance of the SSD, C_P, is magnified by the step-up turn ratio (n) of the transformer, replaced by C_L.

From Fig. 8(b)

$$R_{\text{eq}} = R_P + \frac{R_S}{n^2} \quad X_{\text{eq}} = X_P + \frac{X_S}{n^2} \tag{4}$$

where

$$n = \frac{N_S}{N_P}$$

$$\omega L_M = \frac{\omega C_L R_L^2}{1 + \omega^2 C_L^2 R_L^2} - \omega L_{\text{eq}} \tag{5}$$

$$\omega^2 = \frac{1}{(L_m + L_{\text{eq}})C_L} - \frac{1}{C_L^2 R_L^2} \tag{6}$$

where

$$C_L = n^2 C_P \quad R_L = \frac{R_P}{n^2}.$$

Using an HP 4192A Impedance Analyzer, the small-signal impedance of SSD is measured as 6.3 pF. Likewise, the impedance looking into the primary side of the transformer with the SSD connected to the secondary coil is also measured. Fig. 9 shows the frequency response of this impedance. The resonant frequency is identified as 41 kHz (for clean case), which agrees with (6).

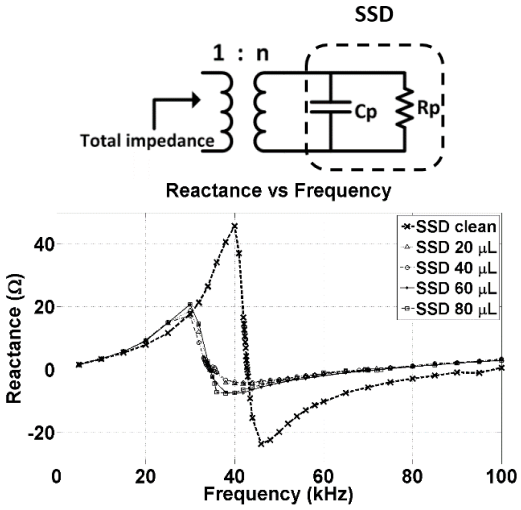

Fig. 9. Total reactance of the transformer and SSD for clean and contaminated cases. Their resonant frequency is the operating frequency of the system, at which the highest output voltage and efficiency is achieved.

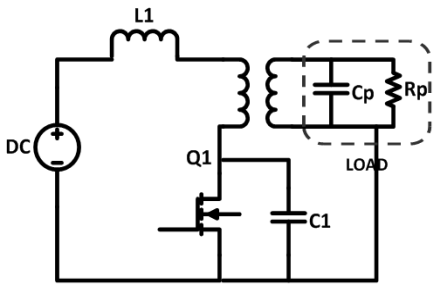

Fig. 10. Schematic of the proposed switching PA.

Fig. 9 also illustrates the resonant frequency for the contaminated case. From Tables I–III, the impedance change due to different volumes of contamination (20–80 μL) is the same. Therefore, the resonant frequency shift is the same regardless of the volume of contamination. The new resonant frequency is shifted to ∼35 kHz. However, in the actual application when sufficient voltage is applied and plasma is generated, the resonant frequency will shift. This impedance change is shown in Fig. 5.

Established from experiments involving different biological samples, the peak-to-peak voltage of v_{SSD} required to achieve proper killing rates is 12 kV. From Fig. 6, the power required is ∼13 W at this voltage level and frequency.

In addition, a scalable system capable of sterilizing a surface of 1 in^2 as well as 4 in^2 or larger is desired. Therefore, a PA that can generate plasma across a 1-in^2 tile is developed and then multiple PAs can be used to drive multiple cells.

Fig. 10 shows the proposed circuit using Class-E topology [22], [23] as the basis, with the load and the transformer achieving resonance to generate plasma across the SSD. This circuit is a dc–ac inverter zero-voltage-switching (ZVS) PA. In this circuit, the transistor is operating as a switch. The current and voltage waveforms of the transistor provide a condition that the high current and the high voltage do not

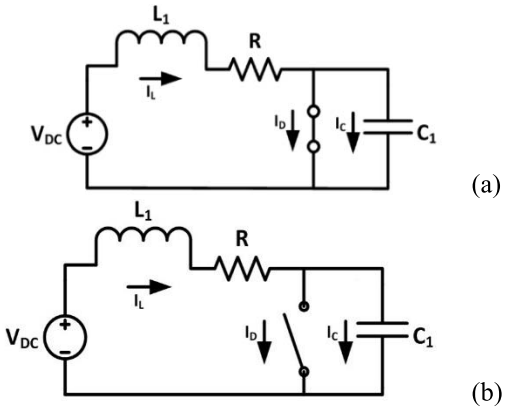

Fig. 11. Equivalent circuit for (a) ON and (b) OFF cases.

overlap, thus minimizing the power dissipation at the transistor and maximizing the efficiency.

The ZVS is achieved by operating the amplifier at an optimum condition [23] by fulfilling

$$v_D(\pi) = 0 \tag{7}$$

$$\frac{dv_D(\omega t)}{dt(\omega t)}|_{\omega t=\pi} = 0. \tag{8}$$

As discussed earlier, the frequency of operation is chosen so that the transformer and the SSD resonate, yielding a high output voltage swing. However, due to the nonlinearity from the transistor, the waveform is not sinusoidal across the RLC tank. The waveform generated is similar to the case presented in [22], where during half of the cycle, the voltage across the RLC tank is the dc source. For this reason, the use of an inductor L_1 is needed. L_1 is located between the dc source and the transformer to obtain a sinusoidal-like waveform across the primary side of the transformer. Due to this inductor, the current will also oscillate across it, becoming reverse in direction in a certain time interval. This may cause a reverse breakdown in the transistor as stated in [15] and the amplifier may fail to function. However, the power MOSFET in use (IRF640ns) has a built-in diode across its source and drain. This diode prevents the reverse breakdown of the transistor and keeps the amplifier from failing.

L_1 and C_1 are evaluated by determining the drain voltage and applying the conditions (7) and (8). First, the circuit is analyzed by applying KVL and KCL. The equivalent circuits are shown in Fig. 11(a) and (b) for both cases when the transistor is turned ON and OFF, respectively.

Following a similar analysis as presented in [23], the component values determined are $L1 = 520\ \mu$H and $C1 = 11$ nF using a resistor value of 75 Ω for R, which is the resistance of the transformer and coil at the operating frequency f of 41 kHz. These were evaluated by applying conditions (7) and (8).

Fig. 12(a) shows the simulated results for the drain voltage v_D. Also, the gate signal v_G is plotted which is a square wave used to turn the transistor ON and OFF at 41 kHz. Fig. 12(b) shows the voltage $v_{\rm PR}$ and current $i_{\rm PR}$ at the primary side of the transformer. To obtain the voltage across the SSD, it is

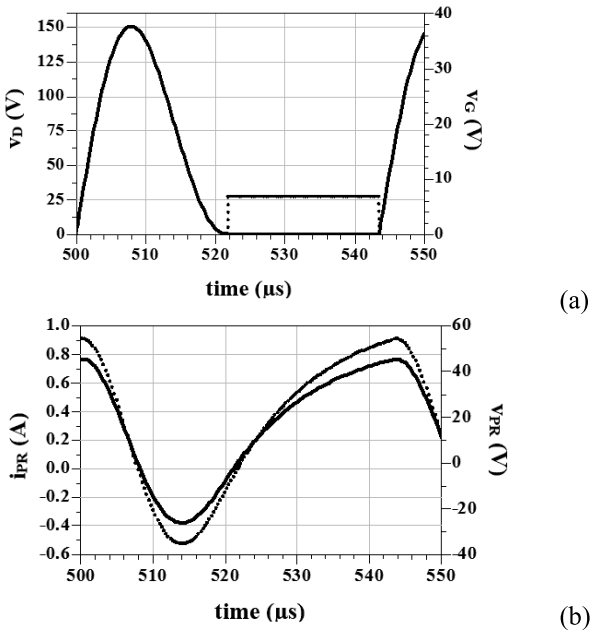

Fig. 12. Simulated results. (a) Drain voltage v_D and driving clock signal v_G. (b) Voltage $v_{\rm PR}$ and current $i_{\rm PR}$ on primary side of transformer. ZVS is achieved, as well as resonance, ensuring high efficiency operation.

multiplied by the number of turns ($n = 165$) of the transformer

$$v_{\rm out} = i_L(t) n R. \tag{9}$$

The results simulated do not take into account the added capacitance from the plasma generated on the surface of the electrode. This will cause a shift in the resonant frequency (Fig. 5). However, using the values at 41 kHz is a good starting point.

IV. System Implementation and Results

A. Clean (Dry) Condition

Using the components derived in the previous section ($L_1 = 520\ \mu$H, $C_1 = 11$ nF), the PA is implemented. The complete circuit consists of voltage regulator, clock generator, optoisolator/gate driver, PA filter, switching PA, and the load (SSD).

The voltage regulator powers up the clock generator and the optoisolator. The optoisolator provides isolation between the PA and the clock source to prevent it from being damaged by current spikes generated at the load. Finally, a PA filter consisting of an inductor and a capacitor are added. This is to prevent any negative current (and voltage) from being fed back to the dc source, which will consist of a battery and may be damaged by such oscillation. The block diagram of the complete system is shown in Fig. 13.

Fig. 14(a) shows the measured voltage $v_{\rm PR}$ and current $i_{\rm PR}$ at the primary side of the transformer. The phase difference between the two waveforms indicates that the system is not operating at resonance. This prevents the system from achieving proper ZVS operation and reaching the desired peak-to-peak voltage of 12 kV across SSD [only 8 kV is attained, as shown in Fig. 14(b)]. However, by gradually changing the frequency, resonance is attained at 34 kHz. New component values using the new frequency are generated. These are

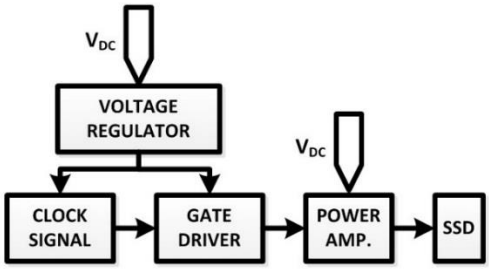

Fig. 13. Complete plasma sterilizer block diagram.

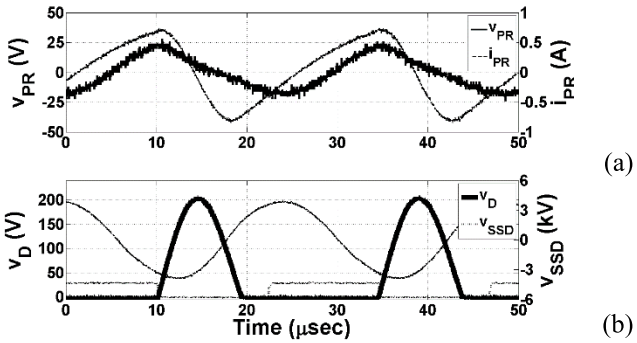

Fig. 14. Nonresonant case at 41 kHz. (a) Current and voltage at primary side of transformer, illustrating presence of reactive component. (b) v_D and voltage across SSD, illustrating failure of achieving 12 kV peak-to-peak. Driving clock signal v_G is also shown.

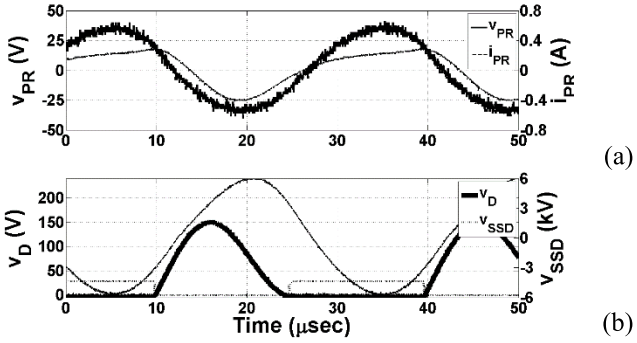

Fig. 15. Resonant case at 34 kHz. (a) In-phase current and voltage at primary side of transformer. (b) v_D and voltage across SSD, achieving perfect ZVS and 12 kV peak-to-peak. Driving clock signal v_G is also shown.

$L_1 = 420$ μH and $C_1 = 21$ nF. Fig. 15 shows the system running at 34 kHz with the new generated components. As illustrated, the impedance seen by the PA is resistive and ZVS is achieved. V_D becomes zero right before the transistor is turned ON, achieving maximum efficiency, and desired peak-to-peak voltage of 12 kV. The total power consumption of the system is 10 W with an efficiency of 91%.

Table IV shows the summary of the result and comparison with previous works that used similar operating frequencies. Compared with those previous published results, this paper achieves the highest voltage and efficiency with power consumption on the same order.

The loss of efficiency in the PA is partially contributed by the parasitics of the inductor and the transformer. The model used to estimate the output power, presented in Section II, does not take into account other parasitic capacitances and phenomena due to plasma generation, which further contributes to the loss of efficiency. Furthermore, the current has random high spikes due to the ionization of the air (Fig. 3), which causes variation of the calculated power. These factors contribute to the 9% loss of efficiency.

TABLE IV
COMPARISON OF PREVIOUS SIMILAR WORK AND THIS PAPER

Reference	Frequency	Peak-to-Peak Voltage	P_{OUT}	Efficiency
[9]	15 kHz	2.8 kV	1 W	50%
[10]	93 kHz	450 V	5 W	67%
[13]	25 kHz	4.6 kV	15 W	88%
[14]	6.2 kHz	2.8 kV	18 W	Not listed
[17]	45 kHz	8 kV	Not listed	Not listed
This work	**34 kHz**	**12 kV**	**10 W**	**91%**

TABLE V
RESONANT FREQUENCY OF SSD AND TRANSFORMER AS A FUNCTION OF VOLTAGE APPLIED

Peak-to-Peak Voltage	Resonant Frequency
8 kV	36.8 kHz
10 kV	34.7 kHz
14 kV	32.5 kHz
15 kV	31.7 kHz

B. Load Variation Due to Voltage and Frequency

As discussed in Section II (Fig. 5), the change in output voltage or frequency will cause the variation of the load impedance at clean (dry) condition. The variation in impedance due to applied voltage change is quite unique to plasma, and was confirmed experimentally. Table V shows the resonant frequency as the peak-to-peak voltage across the SSD is varied from 8 to 15 kV. This shift in frequency results in improper ZVS, which yields to power loss.

C. Contaminated (Wet) Condition

Tables I–III and Fig. 9 show the shift in resonant frequency as the SSD becomes contaminated. This shift in frequency is determined by the way the liquid is placed on the electrode but not the volume of the liquid (Fig. 7). This is confirmed experimentally, shown in Table VI. The 20, 40, 60, and 80 μL of water are applied evenly throughout the surface. It is observed the load varies, shifting the resonant frequency and lowering the voltage across the SSD to ~7.5 kV peak-to-peak. For all four cases in Table VI the results are the same, matching the results observed in Table II. The frequency shift is highly dependent on how the liquid is spread, just as noted in Section II. The new resonant frequency is determined as 29 kHz and new component values of $L_1 = 775$ μH and $C_1 = 15.5$ nF are calculated. At this condition, the system consumes 5.4 W with an efficiency of 88% and an output of 12 kV peak-to-peak.

Now that the operating frequencies have been identified (34 and 29 kHz for clean and contaminated conditions, respectively), the PA must operate within this frequency band.

TABLE VI
RESONANT FREQUENCY OF SSD AND TRANSFORMER AS A FUNCTION OF VOLUME OF WATER APPLIED ON SURFACE. IN ALL CASES, RESULTS ARE THE SAME

Volume	Peak-to-Peak Voltage	Resonant Frequency
20 µL	12 kV	29.1 kHz
40 µL	12 kV	28.9 kHz
60 µL	12 kV	29 kHz
70 µL	12 kV	29.1 kHz

Ideally, this is achieved by using two sets of components, L_1 and C_1, for both conditions. However, this requires more components (switching mechanism), becoming impractical because the end goal is to be able to use multiple identical PAs to power up a larger surface. In addition, the system will have a fixed dc source. As the system is running, and the impedance varies, the same dc input voltage must yield a voltage of at least 12 kV peak-to-peak across the load. The goal is to keep the system as simple as possible.

The best solution is to use the components derived for clean conditions. Under this condition, a voltage of 12 kV peak-to-peak at 34 kHz is achieved. The output power is 10 W with 91% efficiency. Once the surface becomes contaminated, the system changes its frequency to 29 kHz, yielding a peak-to-peak voltage of 16 kV with an output power of 14 W and an efficiency of 83% (keeping dc source constant). However, letting v_{SSD} reach 16 kV peak-to-peak is not desirable. It puts additional stress on the components and affects reliability. In addition, it consumes more power than necessary.

To solve this, the frequency is tuned so a constant amplitude of 12 kV peak-to-peak is maintained throughout the sterilizing process. By doing so, the new operating frequency for contaminated conditions becomes 32 kHz. At this frequency, v_{SSD} is kept at 12 kV peak-to-peak with an output power of 8.6 W and 55% efficiency. Although efficiency has suffered, power consumption has decreased by 39%. This will extend battery life. Therefore, the new frequency band of operation is 32–34 kHz. Table VII compares the two different scenarios with the ideal case.

Fig. 16 shows the complete circuit consisting of a regulator (U1), a clock generator (U2), an optoisolator (U3), a supply filter (U4), and the switching PA. The supply filter is used to prevent any damages to the dc source (battery) from the oscillation of the input current. The size of the system is 2.2-in wide by 3.5-in long.

V. FEEDBACK AND CONTROL FOR LOAD VARIATION

After characterizing the SSD, the resonant points at which plasma is generated are known. These are 34 kHz for clean condition and 29 kHz for contaminated condition (but it is tuned to 32 kHz). As described in the previous section, the dc source stays fixed and only the frequency is varied. It is desired for the controls to do the following:

1) detect surface contamination (impedance variation due to wet surface);
2) adjust frequency as surface is being sterilized (impedance returning to clean state).

TABLE VII
COMPARISON BETWEEN IDEAL AND TWO ALTERNATIVE SOLUTIONS. SOLUTION 2 REQUIRES THE LEAST AMOUNT OF COMPONENTS AND POWER, YIELDING A CONSTANT PEAK-TO-PEAK VOLTAGE OF 12 KV

Scenario	Dry	Dry Eff.	Wet	Wet Eff.
Ideal	10 W	91 %	5.4 W	88%
Dry: 34 kHz, 12 kV peak-to-peak, L_1:420 µH, C_1:21 nF Wet: 29 kHz, 12 kV peak-to-peak, L_1:775 µH, C_1:15.5 nF				
Solution 1	10 W	91 %	14 W	83 %
Dry: 34 kHz, 12 kV peak-to-peak, L_1:420 µH, C_1:21 nF Wet: 29 kHz, 16 kV peak-to-peak, L_1:420 µH, C_1:21 nF				
Solution 2	**10 W**	**91 %**	**8.6 W**	**55 %**
Dry: 34 kHz, 12 kV peak-to-peak, L_1:420 µH, C_1:21 nF Wet: 32 kHz, 12 kV peak-to-peak, L_1:420 µH, C_1:21 nF				

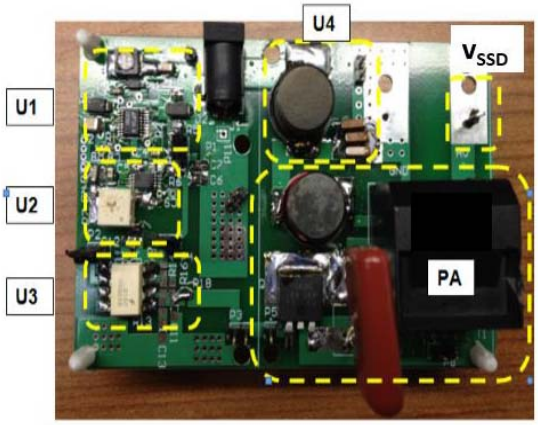

Fig. 16. Complete plasma sterilizer device (without feedback).

Detecting any contamination is accomplished by measuring the voltage v_{SSD} across the SSD. At resonance, the voltage is 12 kV peak-to-peak, but once the surface is contaminated, this reading drops to ∼7.5 kV peak-to-peak. The drop in voltage is significant, making it easy to detect. Once detected, the frequency is decreased until the desired 12 kV peak-to-peak is achieved. As the liquid (contamination) evaporates, the frequency starts increasing, keeping the amplitude of the voltage across the SSD constant.

A. Implementation

Due to the high voltage, direct sampling measurement of v_{SSD} using a microcontroller is not possible. Therefore, v_{SSD} must be stepped down, which can be achieved by using voltage dividers. However, from [25] and (1), the capacitance of the SSD is a function of the voltage across it and the frequency of operation. Once the circuit is out of resonance, the load capacitance changes, making the measurement of v_{SSD} a difficult task. For this paper, the simplest solution is to characterize the load and predetermine the value of V_1 using the voltage divider. This characterization is shown in Fig. 17.

As shown, the value of V_1 does not vary as the frequency changes, making it easier to identify the voltage across the

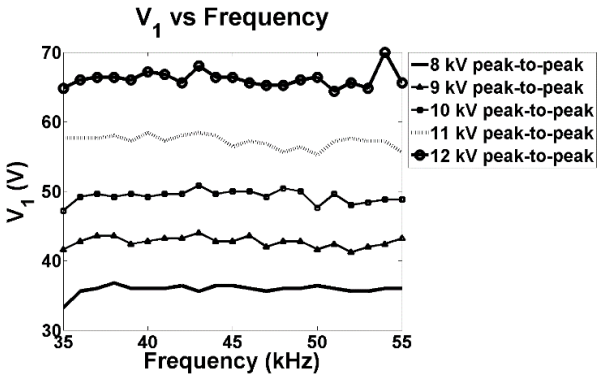

Fig. 17. Peak voltage across the series capacitor as a function of frequency, measured at different peak-to-peak output voltage across the SSD.

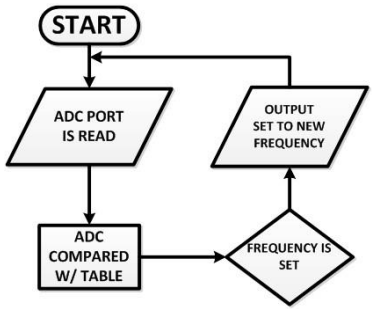

Fig. 18. Microcontroller FC.

SSD regardless of the operating frequency. Finally, a peak detector circuit is used which steps down the voltage V_1 to a manageable range for the microcontroller to read.

Atmel Attiny88 is used as the microcontroller (μC). The output of the peak detector is connected to its ADC port. The voltage value read by the port is compared with a lookup table, which was determined from Fig. 17. The contamination is detected when V_1 drops from 65 to $\sim$32 V. The microcontroller immediately changes the frequency to 32 kHz (output port toggles at 32 kHz). This signal is fed into the gate driver which turns transistor ON and OFF accordingly. As V_1 increases (surfaces is decontaminated), the operating frequency is changed gradually back to 34 kHz. Fig. 18 shows a simple flow chart of the microcontroller.

In addition to monitoring the voltage across the SSD, the input current and the transistor drain voltage can also be monitored. When the system is OFF resonance, the output voltage and the input current drop significantly. For the case when the SSD is clean, the system draws $\sim$260 mA of current, and when it is contaminated, it drops to 85 mA when operating at the same frequency. This change is large enough to be easily detected. Finally, the transistor drain voltage can be monitored to prevent it from exceeding its maximum allowed voltage (200 V). These two, if implemented, can make the feedback more robust.

VI. Conclusion

A PA capable of generating plasma across a capacitive load for sterilization is presented. The PA presented in this paper is robust and simple, providing the necessary output voltage while maintaining a small size (3.5 in $\times$ 2.2 in). Portability is the key factor as well as the ability to handle load variation. This variation is due to the physics of plasma as well as the conditions of the application (clean versus contaminated surface).

The PA yields a constant output peak-to-peak voltage of 12 kV for both clean and contaminated conditions across 32–34 kHz. The system tunes itself by detecting contamination and changing its operating frequency. This is achieved with a feedback mechanism using a microcontroller, which monitors the surface of the SSD throughout the sterilizing process. The maximum output power attained is 10 W with an efficiency of 91%. The PA was designed with scalability for future expansion of the sterilizing area [27].

To further decrease the size of the components, the frequency can be increased and the same design procedure can be applied. The frequency of this paper is constrained by the available transformers, but a custom-built transformer can resonate at a frequency set by the user.

This system may also be used for plasma actuators, ozone generators, or any application that has a capacitive load and requires a high output voltage.

References

[1] N. Mastanaiah, C.-C. Wang, J. Johnson, and S. Roy, "A computational diagnostic tool for understanding plasma sterilization," presented at the 49th AIAA Aerosp. Sci. Meeting, Orlando, FL, USA, 2011.

[2] N. Mastanaiah, U. Saxena, J. Johnson, and S. Roy, "Inactivation of yeast cells using dielectric barrier discharge," presented at the 48th AIAA Aerosp. Sci. Meeting, Orlando, FL, USA, 2010.

[3] M. Laroussi, "Sterilization of contaminated matter with an atmospheric pressure plasma," *IEEE Trans. Plasma Sci.*, vol. 24, no. 3, pp. 1188–1191, Jun. 1996.

[4] J. H. Campos de Souza and J. L. Ferreira, "Development of a corona discharge plasma source for sterilization procedures at atmospheric pressure," in *Proc. IEEE Int. Conf. Plasma Sci. (ICOPS)*, Jun. 2009, p. 1.

[5] K. Kelly-Wintenberg, T. Hontie, A. Hodge, J. Gaskins, J. R. Roth, and Z. Chen, "Mechanism of killing of microorganisms by a one atmosphere uniform glow discharge plasma," in *Proc. IEEE Int. Conf. Plasma Sci. (ICOPS)*, Jun. 1999, p. 202.

[6] K. Stapelmann, N. Bibinov, B. Denis, E. Semmler, and P. Awakowicz, "Sterilization and surface decontamination by a novel VHF-CCP," in *Proc. Abstracts IEEE Int. Conf. Plasma Sci.*, Jun. 2010, p. 1.

[7] S. J. Sung, J. B. Huh, M. J. Yun, B. M. Chang, C. M. Jeong, and Y. C. Jeon, "Sterilization effect of atmospheric pressure non-thermal air plasma on dental instruments," *J. Adv. Prosthodont.*, vol. 5, no. 1, pp. 2–8, Feb. 2013.

[8] Y. Akishev *et al.*, "Atmospheric-pressure, nonthermal plasma sterilization of microorganisms in liquids and on surfaces," *Pure Appl. Chem.*, vol. 80, no. 9, pp. 1953–1969, 2008.

[9] J. M. Alonso, J. Cardesin, E. L. Corominas, M. Rico-Secades, and J. Garcia, "Low-power high-voltage high-frequency power supply for ozone generation," *IEEE Trans. Ind. Appl.*, vol. 40, no. 2, pp. 414–421, Mar./Apr. 2004.

[10] M. Ponce-Silva, J. Aguilar-Ramirez, E. Beutelspacher, J. M. Calderon, and C. Cortes, "Single-switch power supply based on the class E shunt amplifier for ozone generators," in *Proc. IEEE Power Electron. Specialists Conf. (PESC)*, Jun. 2007, pp. 1380–1385.

[11] M. Facta, Z. B. Salam, and Z. B. Buntat, "The development of ozone generation with low power consumption," in *Proc. Innovative Technol. Intell. Syst. Ind. Appl. (CITISIA)*, Jul. 2009, pp. 440–445.

[12] D. Petreus, A. Grama, S. Cadar, E. Plaian, and A. Rusu, "Design of a plasma generator based on E power amplifier and impedance matching," in *Proc. 12th Int. Conf. Optim. Electr. Electron. Equip.*, May 2010, pp. 1317–1322.

[13] M. Akbari, V. Zahedzadeh, S. Shirmohammadzadeh, J. Chitsaz, and M. Chitsaz, "Efficient ozone generator using full-bridge inverter and its performance evaluations," in *Proc. 5th Int. Conf. Power Electron. Drive Syst. (PEDS)*, vol. 2. Nov. 2003, pp. 1182–1187.

[14] J. M. Alonso, J. Garcia, A. J. Calleja, J. Ribas, and J. Cardesin, "Analysis, design and experimentation of a high voltage power supply for ozone generation based on the current-fed parallel-resonant push-pull inverter," in *Proc. Conf. Rec. IEEE, Ind. Appl. Conf., 39th IAS Annu. Meeting*, vol. 4. Oct. 2004, pp. 2687–2693.

[15] J. M. Alonso, C. Ordiz, D. Gacio, J. Ribas, and A. J. Calleja, "Closed-loop regulated power supply for ozone generation based on buck converter and current-fed push-pull resonant inverter," in *Proc. 13th Eur. Conf. Power Electron. Appl.*, 2009, pp. 1–10.

[16] O. Koudriavtsev, W. Shengpei, and M. Nakaoka, "Power supply for silent discharge type load," in *Proc. Conf. Rec. IEEE, Ind. Appl. Conf.*, vol. 1. Oct. 2000, pp. 581–587.

[17] P. Hothongkham, S. Kongkachat, and N. Thodsaporn, "Analysis and comparison study of PWM and phase-shifted PWM full-bridge inverter fed high-voltage high-frequency ozone generator," in *Proc. IEEE 9th Int. Conf. Power Electron. Drive Syst. (PEDS)*, Dec. 2011, pp. 776–781.

[18] M. Balcerak, M. Holub, S. Kalisiak, and M. Zenczak, "High voltage pulse generator using transformer parasitic components for pulsed corona discharge generation," *IEEE Trans. Plasma Sci.*, vol. 41, no. 5, pp. 1587–1593, May 2013.

[19] A. G. Lyublinsky, S. V. Korotkov, Y. V. Aristov, and D. A. Korotkov, "Pulse power nanosecond-range DSRD-based generators for electric discharge technologies," *IEEE Trans. Plasma Sci.*, vol. 41, no. 10, pp. 2625–2629, Oct. 2013.

[20] R. Wu, Y. Wang, Z. Yan, W. Luo, and Z. Gui, "Design and experimental realization of a new pulsed power supply based on the energy transfer between two capacitors and an HTS air-core pulsed transformer," *IEEE Trans. Plasma Sci.*, vol. 41, no. 4, pp. 993–998, Apr. 2013.

[21] A. Suksri, K. Karnchanalekha, K. Tonmitra, and P. Apiratikul, "A comparative study on suitable high voltage sources for ozone generation," in *Proc. 6th Int. Conf. Electr. Eng./Electron., Comput., Telecommun. Inform. Technol.*, 2009, pp. 296–299.

[22] N. O. Sokal, "Class E high-efficiency switching-mode tuned power amplifier with only one inductor and one capacitor in load network-approximate analysis," *IEEE J. Solid-State Circuits*, vol. 16, no. 4, pp. 380–384, Aug. 1981.

[23] M. Kazimierczuk, "Exact analysis of class E tuned power amplifier with only one inductor and one capacitor in load network," *IEEE J. Solid-State Circuits*, vol. 18, no. 2, pp. 214–221, Apr. 1983.

[24] C. H. Li and Y. O. Yam, "Maximum frequency and optimum performance of class E power amplifiers," *IEE Proc. Circuits, Devices Syst.*, vol. 141, no. 3, pp. 174–184, Jun. 1994.

[25] J. M. Alonso, M. Valdes, A. J. Calleja, J. Ribas, and J. Losada, "High frequency testing and modeling of silent discharge ozone generators," *Ozone-Sci. Eng., J. Int. Ozone Assoc.*, vol. 25, pp. 363–376, Oct. 2003.

[26] K. P. Singh and S. Roy, "Impedance matching for an asymmetric dielectric barrier discharge plasma actuator," *Appl. Phys. Lett.*, vol. 91, no. 8, p. 081504, 2007.

[27] R. A. Chinga, S. Roy, J. Lin, and K. Zawoy, "Portable power supply unit for plasma sterilization," U.S. Patent 61 580 083, Dec. 23, 2011.

Raul Andres Chinga (S'08) received the bachelor's degree in electrical and computer engineering and the Ph.D. degree in electrical engineering from the University of Florida, Gainesville, FL, USA, in 2008 and 2013, respectively.

He is currently with Space Systems/Loral, Palo Alto, CA, USA, as an Electric Propulsion Engineer, where he is involved in the development of power electronic products for the generation of plasma for the SPT thrusters installed in commercial satellites. His current research interests include the development of RF switching power amplifiers for applications in plasma generation and wireless power transfer.

Mr. Chinga was a recipient of the Bridge to the Doctorate Fellowship from the University of Florida Graduate School in 2008, the Honorable Mention for the Graduate Research Fellowship from the National Science Foundation in 2010, the Verosi Scholarship from the University of Florida in 2012, and the SEAGEP Fellowship from the University of Florida in 2013.

Jenshan Lin (S'91–M'94–SM'00–F'10) received the Ph.D. degree in electrical engineering from the University of California at Los Angeles (UCLA), Los Angeles, CA, USA, in 1994.

He was with AT&T Bell Labs (which later became Lucent Bell Labs), Murray Hill, NJ, USA, from 1994 to 2001, and with its spinoff, Agere Systems Inc., Inc., Allentown, PA, USA, from 2001 to 2003. In 2003, he joined the University of Florida, Gainesville, FL, USA, where he is currently a Professor. He has authored and co-authored over 230 technical publications in refereed journals and conferences proceedings, and holds 13 U.S. patents. His current research interests include the sensors and biomedical applications of microwave and millimeter-wave technologies and wireless power transfer.

Dr. Lin served as an elected member of the IEEE Microwave Theory and Techniques Society (MTT-S) and Administrative Committee from 2006 to 2011. He was an Associate Editor of the IEEE TRANSACTIONS ON MICROWAVE THEORY AND TECHNIQUES from 2006 to 2010, and is currently the Transactions' Editor-in-Chief. He was a recipient of the 1994 UCLA Outstanding Ph.D. Award, the 1997 ETA KAPPA NU Outstanding Young Electrical Engineer Honorable Mention Award, and the 2007 IEEE MTT-S N. Walter Cox Award.

Subrata Roy received the B.S. degree from Jadavpur University, Kolkata, India, in 1984, and the M.S. and Ph.D. degrees in electrical engineering from the University of Tennessee at Knoxville, Knoxville, TN, USA, in 1990 and 1994, respectively.

He is the Founding Director of the Applied Physics Research Group and an Associate Professor with the Department of Mechanical and Aerospace Engineering, University of Florida, Gainesville, FL, USA. He has co-authored over 150 publications in peer-reviewed journals and bound volumes. He is the inventor of wingless electromagnetic air vehicle, high-power space propulsion device, plasma sterilizer, and 20 other plasma-related inventions.

Dr. Roy is a Distinguished Visiting Fellow with the Royal Academy of Engineering, London, U.K., a fellow of the American Society for Mechanical Engineers, a fellow of the World Innovation Foundation, and an Associate Fellow of the American Institute of Aeronautics and Astronautics. He is a national appointed member and a co-lead of the NATO STO on plasma-based flow control for military air vehicles. He is an Academic Editor of *PLOS-One*.